

Dependence of the final-state effect on the coupling between a CdSe nanoparticle and its neighbors studied with photoemission spectroscopy

Pin-Jiun Wu*

*Department of Electrophysics, National Chiao Tung University, Hsinchu 300, Taiwan
and National Synchrotron Radiation Research Center, Hsinchu 300, Taiwan*

Ku-Ding Tsuei†

*National Synchrotron Radiation Research Center, Hsinchu 300, Taiwan
and Department of Physics, National Tsing Hua University, Hsinchu 300, Taiwan*

Meng-Ting Hsieh and Kung-Hwa Wei

Department of Material Science and Engineering, National Chiao Tung University, Hsinchu 300, Taiwan

Keng S. Liang

*National Synchrotron Radiation Research Center, Hsinchu 300, Taiwan
and Department of Electrophysics, National Chiao Tung University, Hsinchu 300, Taiwan*

(Received 13 September 2006; revised manuscript received 8 January 2007; published 5 March 2007)

A simple model based on an electrostatic calculation of the photoemission effect in the final state is used to characterize the energy shift, relative to bulk material, which is dependent on size in the photoemission spectra of organically passivated CdSe nanoparticles (NPs). For trioctylphosphine oxide/hexadecylamine-passivated NPs, the core-level shifts are well described with a model involving a static effect in the final state. After the NPs are treated with pyridine, the energy shifts are smaller; this decrease is ascribed to a dynamic effect in the final state describing a finite lifetime, on a femtosecond scale, of the photohole residing in the NP. This condition is intimately related to the coupling between the NP and metallic substrate and among NPs themselves. For the valence-band edge, an additional effect of the initial state due to quantum confinement is required to elucidate the energy shift. We find that this initial-state shift is smaller than a prediction according to a semiempirical pseudopotential calculation.

DOI: [10.1103/PhysRevB.75.115402](https://doi.org/10.1103/PhysRevB.75.115402)

PACS number(s): 73.22.-f, 73.90.+f, 79.60.-i

I. INTRODUCTION

Nanoparticles (NPs), which comprise atoms numbering from several tens to thousands, are of great interest in scientific research and technological applications due to a strong correlation between their size and their electronic behavior.¹⁻³ Stable, controllable, and monodispersed NPs offer an opportunity to explore the dimensionally dependent characteristics of materials, such as optical performance, surface effect, and structural dynamics.^{4,5} The various properties of NPs have therefore attracted continuously much intriguing research.

Photoemission spectroscopy is a powerful tool to investigate the electronic structure of nanomaterials.^{1,2} The electron energy measured in a photoemission experiment is, in principle, influenced by effects in both the initial and final states. The initial-state effect is related to the intrinsic electronic properties of materials, while the final-state effect is ascribed to the photohole in the final state and the possible interaction between the outgoing electron and the positively charged state left behind. This charging effect in the final state is related to a quantum phenomenon in single-electron tunneling.

Photoemission spectra of low-dimensional metal clusters dependent on their size have long attracted much attention.^{6,7} The importance of the effect in the final state was demonstrated in such systems, and related calculations were devel-

oped to describe the electronic properties of small clusters.⁸⁻¹⁰ A simple dynamic model that takes into account the finite lifetime of the photohole provides a quantitative interpretation for the photoemission spectra of metallic clusters near the Fermi level; furthermore, the magnitude of the lifetime has been found to depend on the interaction between cluster and substrate.¹¹⁻¹³ In contrast, a detailed investigation of the energy shift, dependent on size, of core-level and valence-band photoemission spectra for semiconductor NPs is lacking. In their pioneer work Colvin *et al.* discussed the relative shift in the valence band among NPs.¹ Other authors subsequently concentrated on the quantum shift, relative to the bulk, of the initial state in the valence-band edge by subtracting the core-level shift.¹⁴ In order to decrease the problem of charging, NPs of thickness less than one monolayer on substrates were used in that work.

In our preceding report of photoemission at high resolution produced with synchrotron radiation, we showed that the core-level shift of CdSe NPs passivated with trioctylphosphine oxide (TOPO)/hexadecylamine (HDA) is satisfactorily described according to a static effect in the final state involving the remaining photohole interacting with the induced polarization, and the valence-band edge shift revealed an additional shift in the initial state due to quantum confinement.¹⁵ Here we report additional data of CdSe NPs treated with pyridine and make a comparison with TOPO/HDA-passivated CdSe NPs. We found that the energy shifts of

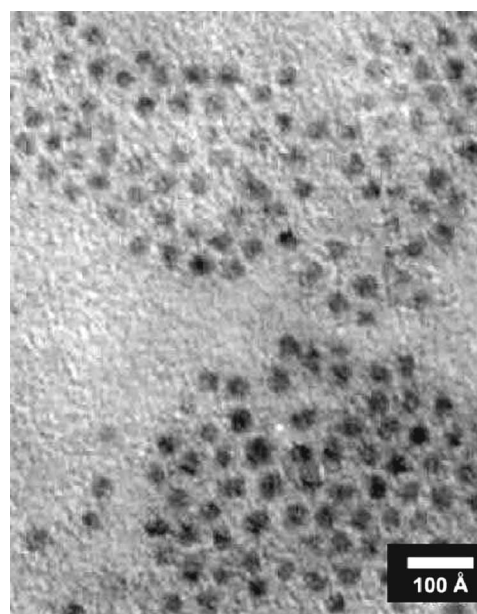
CdSe NPs treated with pyridine, which are smaller than with TOPO/HDA but still considerable, can be related to a dynamic final-state effect, in that the photohole becomes neutralized before the outgoing photoelectron escapes far due to the stronger coupling between NP and the metallic substrate and between particles. We adopt a realistic calculation that considers the inelastic mean free path (IMFP) of photoelectrons and make a comparison with our preceding analysis that involved an assumption of an effective photohole position. Our analysis provides a quantitative understanding of the measured photoemission shift for organically passivated semiconductor NPs. We demonstrate also that the charging effect in the final state in thin multilayer films can be studied in detail without being affected by the macroscopic charging observed in thick insulator samples.

II. EXPERIMENTS

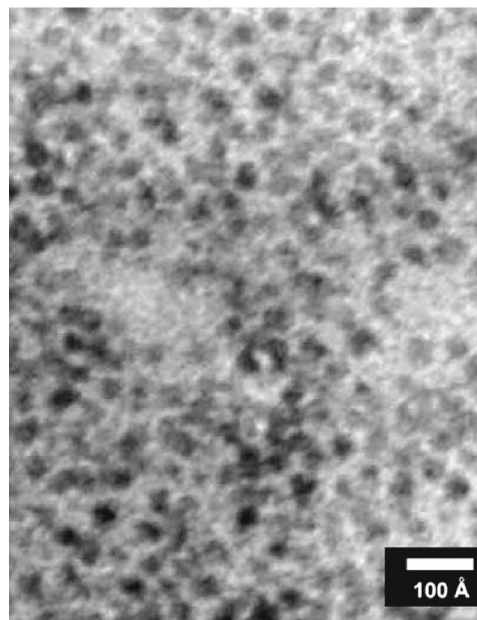
CdSe NPs were synthesized according to a literature method.^{16,17} Briefly, CdO was dissolved in a mixture of TOPO and HDA, and heated to about 270 °C under gaseous argon. Adequate octadecylphosphonic acid (OPA) was injected into the mixture to form the Cd precursor with a color varying from dark red to transparent. The Se solution was prepared on mixing Se pellets with trioctylphosphine (TOP) and maintained at 150 °C; TOPSe was then rapidly injected into the Cd precursor. By controlling the duration of reaction and the growth conditions, CdSe NPs passivated with TOPO/HDA of varied size were obtained. These crude products were dissolved in toluene and methanol to remove the unbound ligands and to improve the size distribution. This purification was repeated several times to achieve CdSe NPs of high quality. CdSe NPs capped with pyridine were obtained on refluxing the TOPO/HDA-passivated CdSe NPs in pyridine for 10–12 h at ~60 °C. After that treatment, the NPs were readily dispersed in pyridine and showed a greatly decreased photoluminescent yield.

In this work we used CdSe NPs of mean diameters D_m in a range 18–42 Å. D_m is defined by $(D_{major} \times D_{minor}^2)^{1/3}$, in which D_{major} and D_{minor} are the major and minor diameters of the prolate particles, respectively. An aspect ratio D_{major}/D_{minor} about 1.2 indicates a nearly spherical shape of these NPs. The diameters of synthesized CdSe NPs, which have a distribution with a standard deviation of about 5%, were determined with x-ray powder diffraction (XPD) and a transmission electron microscope (TEM). TEM images, shown in Fig. 1, reveal that NPs passivated with TOPO/HDA were well separated, while NPs treated with pyridine could touch each other. We verified also the optical-absorption spectra of samples in a solution formed on dispersing NPs (less than 1 mg) passivated with TOPO/HDA and pyridine in toluene and pyridine (3 mL), respectively. We found the relation between the optical-absorption features and the average size to be consistent with the literature.¹⁸

Photoemission experiments using synchrotron radiation were performed at beamlines BL-08A1 and BL-24A1 in the National Synchrotron Radiation Research Center (NSRRC), Taiwan. BL-08A1 is a low-energy beamline with a spherical-grating monochromator (LSGM) that provides radiation with



(a)



(b)

FIG. 1. TEM micrographs of CdSe NPs of mean diameter 32 Å (a) passivated with TOPO/HDA and (b) treated with pyridine.

energy in a range 20–160 eV; we used it to measure valence-band and Se 3*d* core-level spectra. BL-24A1 is a wide-range beamline with a spherical-grating monochromator (WR-SGM) offering photons up to 1500 eV, which we used to measure Cd 3*d* core-level spectra.

All NP samples for the photoemission experiments were prepared on casting a dilute solution with dispersed NPs onto a tantalum foil; the solvent (toluene or pyridine) was allowed to evaporate under gaseous nitrogen. The samples were then transferred to the photoemission chamber within less than 10 min to minimize the possibility of oxidation. The photoemission spectra of samples thus prepared showed no oxidized components from contamination. Pure CdSe powder

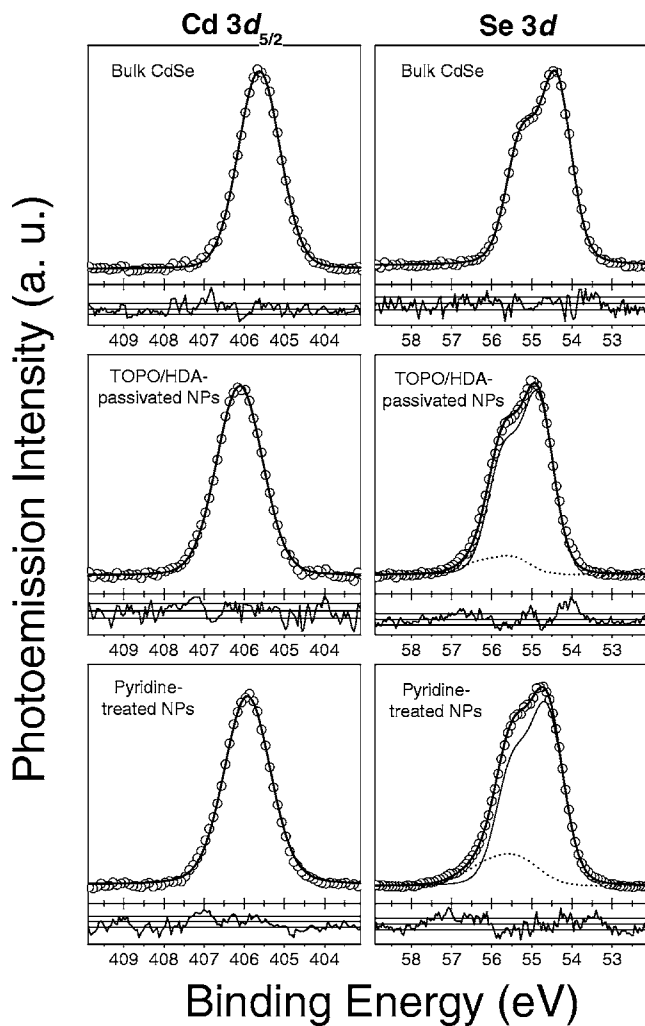


FIG. 2. Core-level photoemission spectra of bulk CdSe and CdSe NPs of mean diameter D_m 32 Å passivated with TOPO/HDA and treated with pyridine. (a) All Cd $3d_{5/2}$ spectra are satisfactorily fitted with a single Voigt component. (b) Se $3d$ spectra are composed of interior (solid curves) and surface (dotted curves) components except for bulk CdSe.

adhered to a Cu foil served as a bulk reference. All NP samples, a bulk sample, and a gold foil were mounted on a grounded sample holder; to calibrate the binding energy, the Fermi level of gold served as a reference. A hemispherical energy analyzer (Omicron EA-125) was used to collect photoelectrons at an overall resolution 0.05–0.1 eV. All photoemission spectra were collected in a normal emission geometry; the base pressure in the chamber was maintained at 2×10^{-9} Torr during the measurements.

III. RESULTS

Figure 2(a) shows Cd $3d_{5/2}$ core-level spectra, measured with a photon energy 480 eV, of bulk CdSe and CdSe NPs, of mean diameter 32 Å, passivated with TOPO/HDA and treated with pyridine, with the corresponding fits. A polynomial background of these spectra was subtracted before fitting the features to the fewest Voigt functions. All Cd $3d_{5/2}$

spectra were fitted with a single Voigt function; hence either the surface component is much smaller than the interior component or the two components of the Cd $3d_{5/2}$ spectra cannot be differentiated in energy.¹⁹ The spectrum of bulk solids shows a binding energy 405.6 eV, in agreement with a value reported in the literature.²⁰ For NP samples the Cd $3d_{5/2}$ spectra are shifted toward higher binding energy relative to the bulk crystallite. The energy shift of NPs passivated with TOPO/HDA is slightly larger than that of NPs treated with pyridine. These spectra notably exhibit line broadening resulting from a finite distribution of size and an increased structural disorder.^{19,21}

Figure 2(b) presents Se $3d$ core-level spectra taken at a photon energy 120 eV; to probe the same depth of the samples, this energy was chosen to obtain a kinetic energy similar to that in the Cd $3d_{5/2}$ core-level spectra. A satisfactory fit was achieved with one single spin-orbit split doublet of Voigt function for the bulk sample. The obtained Se $3d_{5/2}$ feature has a binding energy 54.4 eV, consistent with the literature value.²² In contrast, two spin-orbit split doublets of Voigt functions were necessary to obtain fits of reliable quality for all Se $3d$ core-level spectra of the NP samples. The intensity of the component with higher binding energy increases relative to that of the other component as the particle size decreases.¹⁵ The component at higher binding energy is thus assigned to the surface Se atoms of CdSe NPs because the ratio of surface-to-bulk atoms increases with decreasing size, while the other component arises from interior Se atoms. The surface component of the Se $3d$ core-level spectra of CdSe NPs that exhibits a chemical shift due to unsaturated bonds or bonding to the organic ligands is not discussed here. In contrast, the interior Se $3d$ component has no chemical shift but shows a clear shift to higher binding energy relative to bulk CdSe, with the magnitude of the energy shift comparable to that of the Cd $3d_{5/2}$ core-level spectra.

To examine the passivants, we measured also the P $2p$ and N $1s$ core-level photoemission spectra. The P $2p$ signal of NPs treated with pyridine was much smaller than that of TOPO/HDA-passivated NPs, indicating that pyridine effectively displaced TOPO/HDA on the NP surface. Because we found no N $1s$ signal in the spectrum of NPs treated with pyridine, most pyridine molecules left the NP surface in vacuum, consistent with a report in the literature.²³

Figure 3 shows valence-band photoemission spectra of the same samples as shown in Fig. 2, measured at a photon energy 50 eV so as to have the same probing depth. We verified that the organic compounds contribute to the spectral region below about 5 eV. The first feature below the valence-band edge due purely to NP sharpens with the decreasing size of particles, reflecting an increasing effect of quantum confinement.¹⁵ On extrapolating the linear part just below the edge to its intersection with a linear background, we determined the valence-band edge. For the NP samples the valence-band edges exhibit shifts towards binding energy greater than for the spectrum of a bulk sample. NPs treated with pyridine possess a spectrum in the valence-band range similar to that of NPs passivated with TOPO/HDA, but have a smaller shift of the valence-band edge.

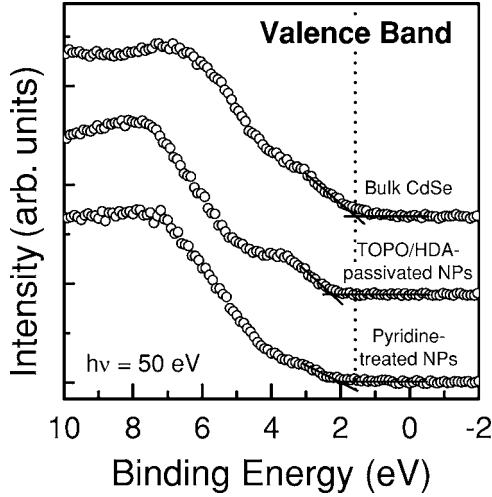


FIG. 3. Photoemission spectra for the valence band of bulk CdSe and CdSe NPs with mean diameter D_m 32 Å passivated with TOPO/HDA and treated with pyridine.

IV. DISCUSSION

A. Core-level shift

According to a three-step model of photoemission, an electron is excited to an unoccupied state leaving a hole; this photoelectron travels to the surface and crosses into vacuum. An electrostatic interaction arises between the outgoing photoelectron and the system left behind, and between the hole and its surrounding medium. The kinetic energy of the outgoing photoelectron is a sum of the photon energy and the total system energy of the initial neutral ground state minus the total system (potential) energy of the final hole state.

Here we consider a classical electrostatic model. Assuming a point charge q at point \vec{r}_q inside a dielectric sphere with a dielectric constant ϵ embedded in vacuum, we solve the electrostatic boundary-value problem at the interface yielding the total potential at point \vec{r} also inside the sphere as

$$\phi_{in} = \frac{q}{\epsilon |\vec{r} - \vec{r}_q|} + \frac{q}{R} \left(\frac{\epsilon - 1}{\epsilon} \right) \sum_{k=0}^{\infty} \frac{k+1}{k(\epsilon+1)+1} \frac{r_q^k}{R^{2k}} r^k P_k(\cos \theta), \quad (1)$$

in which R is the spherical radius, P_k is a Legendre polynomial, and θ is the angle between \vec{r} and \vec{r}_q . The first term is due directly to the point charge while the second term is due to its image, or the induced polarization of the dielectric host because its size is finite. The corresponding potential outside the dielectric sphere is

$$\phi_{out} = q \sum_{k=0}^{\infty} \frac{2k+1}{k(\epsilon+1)+1} \frac{r_q^k}{r^{k+1}} P_k(\cos \theta). \quad (2)$$

This form ensures that the potential vanishes at infinity.

If the photoelectron travels to infinity, there is no interaction between the photoelectron and the remaining system with a photohole. The energy of the final state is the energy

between the photohole and its image. According to Eq. (1) and after rearrangement to facilitate numerical computation, we express the final-state energy as

$$E_f(R, r_h) = \frac{e^2}{2R} \left(\frac{\epsilon - 1}{\epsilon} \right) + \frac{e^2}{2R\epsilon} \left(\frac{\epsilon - 1}{\epsilon + 1} \right) \frac{r_h^2}{R^2 - r_h^2} + \frac{e^2}{2R} \left(\frac{\epsilon - 1}{\epsilon + 1} \right) \sum_{k=1}^{\infty} \frac{1}{k(\epsilon+1)+1} \left(\frac{r_h}{R} \right)^{2k}, \quad (3)$$

in which r_h is the position of the photohole residing in the NP; the factor one half denotes the self energy or the integration of q from 0 to e . Brus formulated an identical expression as the loss of dielectric solvation energy.²⁴ In the limit of a large particle or the bulk ($R \rightarrow \infty$), the first term vanishes. The second term approaches $e^2/(4h)\{(\epsilon-1)/[\epsilon(\epsilon+1)]\}$ for $r_h=R-h$, which is the correct form of image potential at a planar surface. The third term also vanishes as the series approaches $\ln(R)$. As there is no electrostatic energy in the initial neutral ground state, the measured binding-energy shift of the core levels with respect to bulk becomes

$$\Delta E_{CL}(R, r_h) = E_f(R, r_h) - E_f(\infty, r_h). \quad (4)$$

The energy of the final state defined here arises because the organic ligands (TOPO/HDA) with long carbon chains, which passivate the NP surfaces, prevent the photohole from becoming neutralized by an electron tunneling from the metallic substrate before the photoelectron escapes far.²⁵ The bulk CdSe powder sample was, however, not isolated and the photohole was readily neutralized from an electron at the Fermi energy during the photoemission. The associated energy of the final state is thus expected to be minimal, which in the following analysis allows us to take that energy as zero in the bulk limit. The practice justifies this assumption as we subsequently discuss. In the metallic limit as $\epsilon \rightarrow \infty$, the energy of the final state approaches $e^2/(2R)$, the classical charging energy.

In photoemission spectroscopy the primary electron signal becomes attenuated through inelastic scattering as it travels through the interior and then escapes from the surface. The measured energy shift is related to the position of the photohole weighted with an exponential factor describing that attenuation,

$$\Delta E_{CL}(R) = \frac{\int_0^{R-\delta} r^2 dr \int d\Omega E_f(R, \vec{r}_h) e^{-\ell(\vec{r}_h)/\lambda(E_{kin})}}{\int_0^{R-\delta} r^2 dr \int d\Omega e^{-\ell(\vec{r}_h)/\lambda(E_{kin})}}, \quad (5)$$

in which δ denotes the thickness of the surface region not included in the integration, ℓ is the distance for the photoelectron to travel through the dielectric along the normal direction of emission from the position \vec{r}_h of a photohole below the surface, and λ is the IMFP depending on the kinetic energy of the photoelectron. The integration is performed over the whole spherical NP. We consider the surface atoms to be located within half a wurtzite lattice parameter a_w (~ 4.3 Å), which has been used to simulate the diffraction of CdSe nanocrystals on surface relaxation.²⁶ The IMFP is

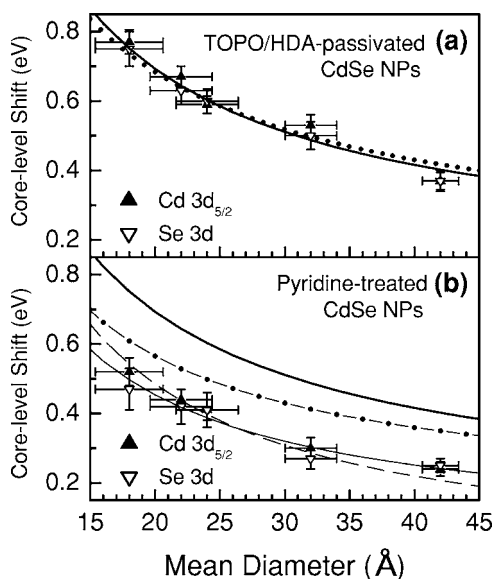


FIG. 4. Energy shifts of the core levels for CdSe NPs (a) passivated with TOPO/HDA and (b) treated with pyridine vs mean diameter, compared with model calculations. The thick solid curve is the shift calculated with Eq. (5) with the position of the photohole weighted by an exponential function describing attenuation; the dotted curve is overplotted according to a simplified model with an effective photohole position for comparison. The dashed curve in (b) is the calculation based on a model for a dynamic effect in the final state that takes into account the lifetime of the photohole. The thin solid and dotted-dashed curves include the contribution from the nearest-neighboring particles with and without considering the dynamic effect in the final state, respectively.

determined according to the “TPP-2M” formula proposed by Tanuma, Powell, and Penn.²⁷ The physical parameters involved in this formula are the density of the solid, the number of valence electrons per atom or molecule, the atomic or molecular mass, and the energy of the band gap. We used 4.66 Å for an IMFP of CdSe obtained with a photoelectron kinetic energy about 60 eV.

Figure 4(a) plots the measured energy shifts, dependent on size, relative to the bulk for Cd $3d_{5/2}$ and the interior component of Se $3d$ core-level spectra of CdSe NPs passivated with TOPO/HDA compared with a calculation (thick solid curve) according to Eq. (5), in which the values of the high-frequency dielectric constant ϵ of CdSe NP dependent on size are obtained from the literature.²⁸ The horizontal error bars specify the full width at half maximum of the size distribution of CdSe NPs, while the vertical error bars indicate the measurement uncertainty. The calculated shifts of the final state without adjustable parameters show satisfactory agreement with the measured energy shifts of the core levels for TOPO/HDA-passivated CdSe NPs with a negligible effect of the final state in the bulk. The magnitude of the Cd $3d_{5/2}$ core-level shift for each size is in general slightly larger than that of the Se $3d$ levels. We attribute this phenomenon to the unresolved Cd $3d$ spectra with the surface Cd contribution that is weighted more to the shift of the final state. To avoid divergence in our classical model, a finite surface thickness δ must be included in Eq. (5).

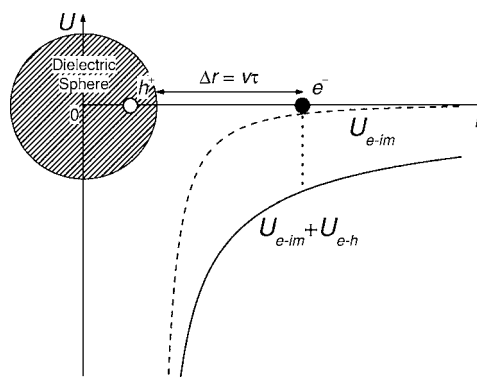


FIG. 5. Schematic diagram of the dynamic effect in the final state illustrates the electrostatic potential-energy curve as the photoelectron travels to infinity at which the zero energy is defined. In the presence of the photohole, the potential energy is the sum of the electron-hole energy (U_{e-h}) and the electron-image energy (U_{e-im}) following the solid curve. If the photohole becomes neutralized when the photoelectron travels to $R+v\tau$ the potential energy transfers to the dashed curve as only the electron-image energy remains.

A simplified model calculation undertaken in our preceding work,¹⁵ in which we considered an effective photohole position $r_h=R-h$ as the fitting parameter for the experimental data, is plotted as the dotted curve in Fig. 4(a) for comparison. A slightly poorer fit than through use of Eq. (5) is obtained with $h=3.6$ Å. This value is reasonable, since it is close to the IMFP of 4.66 Å. The simpler model for an effective photohole position provides a satisfactory approximation to the more complicated spherical IMFP model.

Using the same parameters, we calculated the bulk term $E_f(\infty, r_h)$ considering the IMFP to be 0.088 eV, which would yield a constant downward shift of the calculated curve in Fig. 4(a), apparently deviating from the measured energy shift. If one retains the bulk term while treating the IMFP and the surface thickness as fitting parameters, the resulting fit is much poorer and has an unrealistically large IMFP and an unphysically small surface thickness. Including the bulk term in the effective photohole position model results in a poor fit with an unrealistic photohole position $r_h=R-0.8$ Å. These results support our assumption to neglect the bulk effect in the final state.

Figure 4(b) shows the energy shifts of CdSe NPs treated with pyridine with respect to bulk CdSe, which are always smaller than those of NPs passivated with TOPO/HDA. To explain the energy shifts of NPs treated with pyridine, we introduce a dynamic effect in the final state: i.e., the photohole becomes neutralized while the photoelectron is still in a region near the NP surface before it escapes far or to infinity.¹¹

A schematic diagram describing the effect of a dynamic final state is illustrated in Fig. 5, in which is drawn the electrostatic potential energy of the photoelectron as a function of its position outside the dielectric sphere. The zero potential energy is defined as the photoelectron approaches infinity. In the presence of the photohole, the potential energy is the sum of contributions from the induced image and the photohole following the solid curve. If the photohole becomes neutralized when the photoelectron travels to $R+v\tau$,

the potential energy of the photoelectron transfers to the dashed curve as only the image potential energy remains. Work needed to be done to remove the photoelectron to infinity is thus decreased by the interaction energy of the electron and hole, deduced from Eq. (2),

$$E_{e-h}(R, \vec{r}) = \frac{e^2}{|\vec{r}_e - \vec{r}_h|} \left(\frac{2}{\epsilon + 1} \right) + \frac{e^2}{r_e} \left(\frac{\epsilon - 1}{\epsilon + 1} \right) + \frac{e^2}{r_e} \left(\frac{\epsilon - 1}{\epsilon + 1} \right) \sum_{k=1}^{\infty} \frac{1}{k(\epsilon + 1) + 1} \left(\frac{r_h}{r_e} \right)^k P_k(\cos \theta), \quad (6)$$

in which $\vec{r}_e = \vec{R} + \Delta\vec{r}$ with $\Delta\vec{r} = \vec{v}_\ell \tau$, \vec{v}_ℓ is the velocity of the photoelectron towards the analyzer, and θ is the angle between \vec{r}_e and \vec{r}_h . In this model, for simplicity we take τ as an average relaxation time instead of the characteristic time in the tunneling probability used in Ref. 11. When the dielectric constant approaches infinity, the total energy shift based on the effect of the dynamic final state is given by $\lim_{\epsilon \rightarrow \infty} [\Delta E_{CL}(R) - E_{e-h}(R, r)] = e^2 [1/(2R) - 1/r]$, closely resembling a model proposed for metallic clusters on a graphite substrate.¹¹

A fit of the formula $\Delta E_{CL}(R) - E_{e-h}(R, r)$ to the core-level energy shifts of CdSe NPs treated with pyridine is shown in Fig. 4(b) as the dashed curve. The experimental results are satisfactorily described with our model with a parameter $\Delta r = 68 \text{ \AA}$. Hence the outgoing photoelectron maintains an interaction with the photohole left behind in the NP until it travels 68 \AA from the surface. The photoelectron leaves the NP with a kinetic energy about 60 eV for the Se $3d$ level, corresponding to a velocity $\vec{v}_\ell = 4.6 \times 10^6 \text{ m/sec}$. The lifetime of the photohole left in the dielectric particle is thus $\tau = 1.48 \times 10^{-15} \text{ s}$, but the smallest and largest NP data show a perceptible deviation from the model fitted curve (dashed curve).

We further consider the influence of the nearest-neighbor particles as a correction because the interparticle distances were small for NPs treated with pyridine [see Fig. 1(b)]. An additional interaction between the remaining photohole and the induced image charges in the neighboring NPs can diminish the apparent energy shift in the final state. The TEM images showed an arrangement of nearly hexagonal close-packed NPs. We estimate from, for example, Fig. 1(b) that, on average, one NP in the surface layer of a film had four neighboring NPs nearly in contact, but maintained a distance $\sim 15 \text{ \AA}$ surface to surface from the other five nearest neighbors, because of remaining TOPO/HDA surfactants on the NP surface.^{23,29} For simplicity we assume that the remaining photohole was effectively located at the center of the NP and interacted with the induced image charges of all nearest-neighbor NPs. The final-state shift after this correction for the nearest neighbors is shown as the dotted-dashed curve in Fig. 4(b). An additional decrease is clearly required, which is again due to the dynamic effect in the final state. The best fit including both the dynamic effect in the final state and the correction for the nearest neighbors is plotted as a thin solid curve in Fig. 4(b), showing satisfactory agreement with data points of all sizes. In this fit, Δr

$= 128 \text{ \AA}$ or $\tau = 2.78 \times 10^{-15} \text{ s}$. This value is expected to correspond to the upper limit of the lifetime, as most photoholes are created near the NP surface leading to a smaller contribution from neighboring particles than our assumption at the center. The interaction between photoelectron and image becomes small for $\Delta r > 30 \text{ \AA}$, because of its dipolar character, and is almost negligible in the above-mentioned dynamic effect and the correction due to nearest neighbors. For NPs passivated with TOPO/HDA, the mean distance surface to surface between NPs was $\sim 15 \text{ \AA}$. The energy shifts are thus decreased by $0.02\text{--}0.04 \text{ eV}$ considering the contribution from the neighbors, which is insignificant to affect our conclusion.

We attribute the dynamic effect in the final state of CdSe NPs treated with pyridine to the distinct coupling strength between NP and metallic substrate and between particles from TOPO/HDA-passivated NPs. TOPO and HDA molecules with long carbon chains that are attached to the NP surface via their lone pairs can prevent the particles from being in contact. In contrast, pyridine is unstable to adsorption on the NP surface in vacuum, leaving the NP partially uncovered with a smaller distance between the NP and the metallic substrate and between the NPs themselves. We expect that the coupling in the latter system is stronger than that in the former, resulting in a larger probability of electron tunneling and a smaller lifetime of the remaining photohole in the NP. Our estimate shows the photohole lifetime to be in a range $1.5\text{--}2.8 \times 10^{-15} \text{ s}$ for NPs treated with pyridine. Accordingly the dynamic effect of the final state cannot be ignored for a system with strong interactions between a dielectric particle and a metallic substrate and between particles. For comparison, the dynamic effect in the final state has been observed in naked Ag NPs (Ref. 11) and in Ag and Au NPs passivated with alkanethiolate supported on a graphite surface^{12,13} with a photohole lifetime $0.2\text{--}0.5 \times 10^{-15} \text{ s}$, smaller than our case.

B. Valence-band edge shift

The measured shifts of the valence-band edge of CdSe NPs passivated with TOPO/HDA are presented in Fig. 6(a). The valence-band edge shift is invariably larger than the core-level shift. The final-state shift of the valence-band edge is expected to differ from that of the core levels because the wave function of the valence-edge hole penetrates more deeply into the interior of the NP.²⁸ Following Ref. 24, we model the hole $1S$ wave function with, for simplicity, $\sin(\pi r/R)/r$ as in an infinite well. This approximation was used in Ref. 28 to obtain the dielectric constant and exciton energy. The average shift of the final state with the same IMFP is shown as the dotted curve. For a step well the hole wave function is expected to have greater weight near the surface. The pure effect of the final state evidently underestimates the valence-band edge shift. We expect an additional shift due to quantum confinement as the effect of the initial state. The simplest form is the kinetic-energy term in a quantum-confinement well as described by Brus,³⁰ which has been used with qualitative success to explain the shift in CdS NPs.¹ Wang and Zunger calculated the electronic structure of

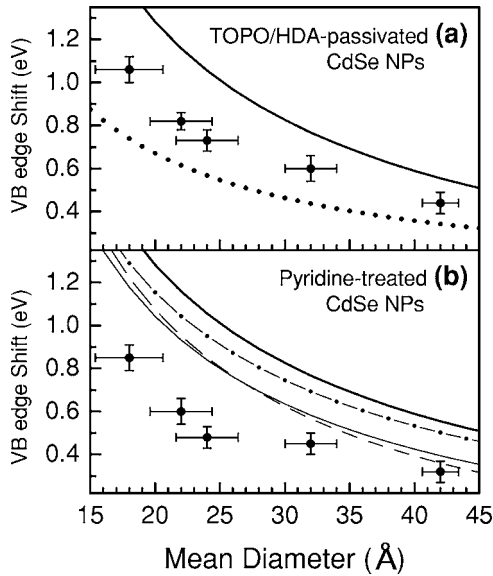


FIG. 6. Energy shifts of the valence-band edge for CdSe NPs (a) passivated with TOPO/HDA and (b) treated with pyridine vs the mean diameter, compared with model calculations. The dotted curve indicates the calculated final-state shift weighed with a 1S wave function considering the IMFP, and the thick solid curve includes an additional quantum shift [Eq. (7)] reported in Ref. 28. The dashed curve in (b) results from a calculation based on a model for the dynamic effect in the final state with the same parameter used in Fig. 4(b). The thin solid and dotted-dashed curves specify the total shift including the contribution from the nearest-neighboring particles with and without the dynamic final-state effect, respectively.

surface-passivated wurtzite CdSe quantum dots using a semi-empirical pseudopotential method (SEPM).²⁸ They showed that the valence-band maximum shifts to smaller energy relative to bulk CdSe as the NP becomes smaller.

A correct description of the total shift of the valence-band edge with particle size includes shifts for both the initial and final states as

$$\Delta E_{VB} = \Delta E_{SEPM}(R) + \overline{\Delta E_f(R)}, \quad (7)$$

in which $\Delta E_{SEPM}(R)$ is extracted from the predicted energy shifts with size by SEPM (Ref. 28) and $\overline{\Delta E_f(R)}$ is the average of Eq. (3) over the wave function of the hole in the NP considering the IMFP.^{1,24} The thick solid curve in Fig. 6(a) is the plot of Eq. (7) using the wave function for an infinite well. It appears to overestimate the measured shifts, and this overestimate becomes worse for smaller NPs. We emphasize here that the amount of the shift for the final state differs in the core levels and the valence-band edge such that to extract the shift of the initial state dependent on size or the quantum confinement by simply subtracting the core-level shift from the valence-band edge shift can yield an underestimate for the larger NPs.¹⁴ Including the IMFP in the calculation of the shift for the valence-band final state produces a minute increase about 0.02 eV; thus a simpler calculation without it is sufficient.

Figure 6(b) shows the valence-band edge shifts of CdSe NPs treated with pyridine compared with the calculation based on the model for a dynamic effect in the final state with the same parameters as for the corresponding core-level shift. We considered also the contribution from the nearest-neighboring particles (dotted-dashed and thin solid curve). The calculation evidently overestimates the measurement. The deviation is similar to that in Fig. 6(a).

Several reasons underlie this deviation. One might suspect an approximation of a NP of prolate shape (aspect ratio 1.2–1.3) by a sphere to result in an error in the initial-state calculation, but the deviation of a prolate spheroid from the averaged sphere invariably produces an increase of quantum confinement and a larger shift in the initial state, contrary to the experimental observation. Another point is the presence of stacking faults in NP that have been experimentally observed,¹⁶ but a calculation of CdSe quantum dots in both wurtzite and zinc-blende structures shows no significant alteration of exciton energies.³¹ Stacking faults thus seem unable to explain such a discrepancy. A third possibility is that a lattice contraction up to 1% and structural disorder were observed experimentally²¹ while the calculation assumes a truncated bulk with a bulk lattice parameter. According to a theoretical investigation of CdS clusters, the band gap is decreased 0.11 eV assuming 1.4% lattice contraction.³² This effect might explain the discrepancy between experiment and theory.

V. CONCLUSION

We have investigated the energy shift dependent on the size of the core levels and valence-band edge for organically passivated CdSe NPs of various diameters. For NPs passivated with TOPO/HDA the core-level shifts are satisfactorily described with a model of a static final state based on an electrostatic interaction between the photohole and the dielectric background, including the inelastic mean-free-path effect of the photoelectron, with no adjustable parameter. For NPs treated with pyridine, the energy shifts are smaller. A dynamic model characterizing the finite lifetime of the photohole on a femtosecond scale is invoked to elucidate these energy shifts considering the interaction between photoelectron and photohole. For the valence-band edge an additional shift in the initial state due to quantum confinement is required to explain the data. A pseudopotential calculation of the valence-band edge shift in the literature appears to overestimate the effect in the initial state compared to our experimental observation. The discrepancy might reflect a lattice contraction in the NP that was neglected in the calculation.

ACKNOWLEDGMENTS

One of us (P.J.W.) is grateful to Tun-Wen Pi, Yaw-Wen Yang, and Chien-I Ma for assistance with the photoemission experiments. National Science Council of Taiwan supported this work under Grants No. NSC 94-2122-M-213-017 and No. NSC 94-2112-M-213-016.

*Electronic address: pinjiun.ep89g@nctu.edu.tw

†Author to whom correspondence should be addressed. Electronic address: tsuei@nsrrc.org.tw

- ¹V. L. Colvin, A. P. Alivisatos, and J. G. Tobin, *Phys. Rev. Lett.* **66**, 2786 (1991).
- ²P. Zhang and T. K. Sham, *Phys. Rev. Lett.* **90**, 245502 (2003).
- ³H. Mattoussi, L. H. Radzilowski, B. O. Dabbousi, E. L. Thomas, M. G. Bawendi, and M. F. Rubner, *J. Appl. Phys.* **83**, 7965 (1998).
- ⁴H. Borchert, D. V. Talapin, N. Gaponik, C. McGinley, S. Adam, A. Lobo, T. Moller, and H. Weller, *J. Phys. Chem. B* **107**, 9662 (2003); J. Rockenberger, L. Troger, A. Kornowski, T. Vossmeyer, A. Eychmuller, J. Feldhaus, and H. Weller, *ibid.* **101**, 2691 (1997).
- ⁵E. Rabani, B. Hetenyi, B. J. Berne, and L. E. Brus, *J. Chem. Phys.* **110**, 5355 (1999); C. McGinley, M. Riedler, T. Moller, H. Borchert, S. Haubold, M. Haase, and H. Weller, *Phys. Rev. B* **65**, 245308 (2002).
- ⁶K. S. Liang, W. R. Salaneck, and I. A. Aksay, *Solid State Commun.* **19**, 329 (1976).
- ⁷H. G. Boyen, A. Ethirajan, G. Kästle, F. Weigl, P. Ziemann, G. Schmid, M. G. Garnier, M. Büttner, and P. Oelhafen, *Phys. Rev. Lett.* **94**, 016804 (2005).
- ⁸G. K. Wertheim, S. B. DiCenzo, and S. E. Youngquist, *Phys. Rev. Lett.* **51**, 2310 (1983).
- ⁹G. Makov, A. Nitzan, and L. E. Brus, *J. Chem. Phys.* **88**, 5076 (1987).
- ¹⁰M. Seidl, K. H. Meiwes-Broer, and M. Brack, *J. Chem. Phys.* **95**, 1295 (1991).
- ¹¹H. Hovel, B. Grimm, M. Pollmann, and B. Reihl, *Phys. Rev. Lett.* **81**, 4608 (1998).
- ¹²A. Tanaka, Y. Takeda, T. Nagasawa, and S. Sato, *Phys. Rev. B* **67**, 033101 (2003); A. Tanaka, Y. Takeda, M. Imamura, and S. Sato, *ibid.* **68**, 195415 (2003).
- ¹³M. Imamura and A. Tanaka, *Phys. Rev. B* **73**, 125409 (2006).
- ¹⁴T. van Buuren, L. N. Dinh, L. L. Chase, W. J. Siekhaus, and L. J. Terminello, *Phys. Rev. Lett.* **80**, 3803 (1998).
- ¹⁵P. J. Wu, K. D. Tsuei, K. H. Wei, and K. S. Liang, *Solid State Commun.* **141**, 6 (2007).
- ¹⁶C. B. Murray, D. J. Norris, and M. G. Bawendi, *J. Am. Chem. Soc.* **115**, 8706 (1993).
- ¹⁷P. Reiss, J. Bleuse, and A. Pron, *Nano Lett.* **2**, 781 (2002).
- ¹⁸W. W. Yu, L. Qu, W. Guo, and X. Peng, *Chem. Mater.* **15**, 2854 (2003).
- ¹⁹H. Borchert, D. V. Talapin, C. McGinley, S. Adam, A. Lobo, A. R. B. de Castro, T. Moller, and H. Weller, *J. Chem. Phys.* **119**, 1800 (2003).
- ²⁰S. W. Gaarenstroom and N. Winograd, *J. Chem. Phys.* **67**, 3500 (1977).
- ²¹K. S. Hamad, R. Roth, J. Rockenberger, T. van Buuren, and A. P. Alivisatos, *Phys. Rev. Lett.* **83**, 3474 (1999).
- ²²E. Agostinelli, C. Battistoni, D. Fiorani, G. Mattogno, and M. Noguez, *J. Phys. Chem. Solids* **50**, 269 (1989).
- ²³J. E. Bowen Katari, V. L. Colvin, and A. P. Alivisatos, *J. Phys. Chem.* **98**, 4109 (1994).
- ²⁴L. E. Brus, *J. Chem. Phys.* **79**, 5566 (1983).
- ²⁵If the (insulating) films are too thick, the electron-tunneling time or photohole lifetime becomes too long compared to the time until the next photoionization event. As a result, macroscopic charging is observed with a large shift proportional to the photon flux. To avoid this unwanted phenomenon, we used a highly dilute solution to prepare thin multilayer films.
- ²⁶M. G. Bawendi, A. R. Kortan, M. L. Steigerwald, and L. E. Brus, *J. Chem. Phys.* **91**, 7282 (1989).
- ²⁷S. Tanuma, C. J. Powell, and D. R. Penn, *Surf. Interface Anal.* **21**, 165 (1993).
- ²⁸L. W. Wang and A. Zunger, *Phys. Rev. B* **53**, 9579 (1996).
- ²⁹B. S. Kim, L. Avila, L. E. Brus, and I. P. Herman, *Appl. Phys. Lett.* **76**, 3715 (2000).
- ³⁰L. E. Brus, *J. Phys. Chem.* **90**, 2555 (1986).
- ³¹B. Zorman, M. V. Ramakrishna, and R. A. Friesner, *J. Phys. Chem.* **99**, 7649 (1995).
- ³²M. V. Rama Krishna and R. A. Friesner, *J. Chem. Phys.* **95**, 8309 (1991).